Real Time Model-Based Monitoring of a PEM Fuel Cell Flooding And Drying Out

Nicolas Fouquet
PSA Peugeot Citroën
Centre Technique de Carrières sous Poissy
212, bd Pelletier, CI29
78307 Carrières sous Poissy, France
Email : nicolas.fouquet@mpsa.com

***Abstract*—The present paper deals with real time monitoring of flooding and drying out of a proton exchange membrane (PEM) fuel cell using a model-based approach coupled with voltage and current dynamic measurements. The model used in this study is inspired by the Randles equivalent electrical circuit. It was found that monitoring the evolution of the three resistances of this modified Randles model was an efficient and robust way of monitoring the state-of-health of the fuel cell stack. Fitting of the model parameters to experimental data is investigated both in the time domain, using a linear recursive least square algorithm, and in the frequency domain, using a non-linear least square Levenberg-Marquardt algorithm. A study of the voltage response of a 220cm^2, 6-cell, air/H_2 PEM fuel cell to a square current signal is carried out, in order to assess the performances of the different methods.**

I. INTRODUCTION

From an automotive manufacturer point of view, fuel cells have evolved, over the past decade, from a laboratory experiment to one of the potential successors to the internal combustion engine. Now that vehicle integration has been demonstrated and performances are ramping up, command and control issues as well as Fault Detection and Isolation (FDI) gather more importance to the day.

FDI procedures consist of comparison between the actual process behavior and the theoretical reference process behavior given by a model. The detection and isolation of the plant faults mainly consists of two steps. The first step provides the possible inconsistencies between the process model and its actual behavior. The second step is the decision procedure for diagnosis which allows locating or isolating the fault and possibly identifying its origin. Robust detection schemes aim at minimising false alarm and non-detection. According to the knowledge and the quality of data available for the process under diagnostic, the monitoring methods used are mainly based on two approaches: model-based and non-model-based. Further subclassifications and detailed reviews on each approach are given in [1]. On one hand the main drawback of the non-model based methods consist in the fact they need a recognition pattern step which is very difficult, as it requires exactly identical operating conditions and exact reproduction of faults: Failure scenarios for training are needed. On the other hand, concerning the model based method, the FDI performances depend on the accuracy of the model. The Fuel cell system is a complex non stationary process. Obtaining the analytical dynamic model is a difficult task. In the present paper an approach based on the Randles model structure is used.

One of the major challenges in proton exchange membrane fuel cell FDI and control reconfiguration lies in the state of hydration of the membrane electrode assembly [2]. In a PEM fuel cell, the electrolyte is a polymer membrane that ensures proton conductivity between anode and cathode while being electronically insulated. Protons are able to cross the membrane only if attached to water molecules. Thus, it is of prime importance to ensure at all time a steady minimum water content in the electrolyte. To do so, water vapor is usually added to the feed stream, which can be quite a tricky task to achieve properly, for the following reasons :

1) relative humidity sensors only measure the inlet/outlet water content of the gases, which are not straightforwardly linked to the state of hydration of the membrane electrode assembly [3].
2) actuators, among which we can cite enthalpy wheels, gas/gas or water/gas membrane humidificator are often slow and/or inaccurate.

These technical shortcomings can lead to too much or too few water being injected in the fuel cell, which in turn causes flooding or drying out. Prolonged operation in either of these two states can be very harmful, or even fatal, to the stack [4].

The challenge of monitoring water distribution within a PEM fuel cell has been taken up by many research teams around the world over the past couple of years. Good results were obtained by using transparent bipolar plates [5], gas chromatography [6], or even neutron imaging [7]. However efficient they might be, it is very unlikely that these methods will ever find their way into mass production.

Softer methods were thus also developed, which focus on the monitoring of data closely related to the state of hydration of the membrane electrode assembly. Pressure drop across the cathode compartment [8], [9], as well as current/voltage characteristics [10] were for instance studied. These methods make use of sensors already available on the fuel cell system, and rely on signal processing to monitor the state-of-health (SOH). Voltage measurement is one of the most interesting method as it appears to be the only variable allowing a

978-1-4244-8218-4/10/$26.00 ©2010 IEEE

measurement at the cell level while still being non intrusive. In [10], the diagnosis solely depends on the processing of steady-state current/voltage data. This proves to be efficient as far as fault detection is concerned, but leads to an indetermination when it comes to fault isolation since flooding and drying out both cause a voltage drop. To overcome this problem, the decision stage of the algorithm makes use of the first derivative of a voltage related fault indicator, assuming that the dynamic behavior of this indicator over the time period during which the failure occurred is always sufficiently different between flooding and drying out.

The study presented in this article focuses on the problem of real-time monitoring of the water content of PEM fuel cells through voltage and current measurements under dynamic conditions. In [3], we showed how a model-based approach coupled with electrochemical impedance spectroscopy (EIS) measurements could help identify a set of parameters exhibiting a much greater sensitivity and selectivity to flooding and drying than the voltage does. As a first step toward on-board integration, we will show here that this approach remains fully functional when real-time imperatives are considered. This article is organized as follows : section II briefly presents the fuel cell impedance model developed in [3]. So as to achieve real time fault detection and isolation, a time domain recursive least square scheme is first investigated in section III, in conjunction with a linear discrete model of the fuel cell, derived from the non-linear one presented in section II. Although theoretically sound, this approach raises practical shortcomings which led us on to considering a fitting scheme operating in the frequency domain, developed in section IV. Experimental results are then given in section V.

II. FUEL CELL IMPEDANCE MODEL

The Randles cell, is a common and practical way of modeling an electrochemical electrode as an equivalent circuit. It consists of four elements : two resistors, R_m, standing for the ohmic resistance of the electrolyte, here the proton exchange membrane, and R_p standing for the polarisation resistance, due to the oxygen reduction reaction ; a plane capacitor, C_{dl}, representing the double layer capacitance at the electrode/electrolyte interface ; and a Warburg diffusion element.

From the Butler-Volmer equation and Fick's second law of diffusion, it is possible to derive the general expression of the diffusion impedance for a finite length diffusion layer, Z_δ [11] :

$$Z_\delta = R_d \frac{\tanh\sqrt{\tau_d j\omega}}{\sqrt{\tau_d j\omega}} \tag{1}$$

where τ_d is dimensionally homogenous to a time $[s]$ and R_d is dimensionally homogenous to an electrical resistance $[\Omega]$ [3].

By further making the assumption that the rate limiting reaction is the oxygen reduction at the cathode, we will neglect the contribution of the anode impedance to the cell impedance. The impedance of the Randles cell is thus :

$$Z_{randles}(j\omega) = R_m + \frac{1}{j\omega C_{dl} + \frac{1}{R_p + Z_\delta}} \tag{2}$$

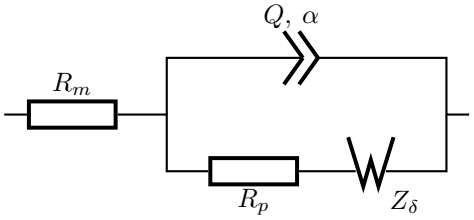

Fig. 1. Randles cell with CPE.

Moreover, it was shown in [3], that replacing the standard plane capacitor by a constant phase element (CPE) allowed for a much better fit between experimental data and model. Thus, the equivalent circuit selected to model our fuel cell is that of figure 1, and the overall impedance is :

$$Z(j\omega) = R_m + \frac{1}{(j\omega)^p Q + \frac{1}{R_p + Z_\delta}} \tag{3}$$

As reported in [3], the non-integer power of the CPE was found to be statistically constant over a wide range of operating conditions, thus comforting the assumption that it has a physical meaning. It was also showed that monitoring the evolution of the three resistances (R_m, R_p and R_d) of this modified Randles model was an efficient and robust way of monitoring the state-of-health of the fuel cell stack.

III. FITTING IN THE TIME DOMAIN

Fitting in the time domain using a recursive algorithm is well suited for real time operating mode since the parameters estimation, and hence the diagnosis, can be updated with each new measured sample. On the downside, these algorithms only operate on linear models.

A. Model linearization and simplification

The model developed in section II is non linear due to the Warburg impedance and exhibits a non integer order because of the CPE. As a first approximation, we will abandon the CPE and reverse to the traditional Randles cell. Considering the diffusion process is mainly a low frequency phenomenon, the non-linearity of the Warburg impedance can be dealt with using a Taylor development. A first order development of the concentration-diffusion impedance expression as given by Eqn. 1 yields for low frequencies :

$$\lim_{\omega\to 0} Z_\delta(j\omega) = R_d \frac{1 + \frac{\tau_d j\omega}{6}}{1 + \frac{\tau_d j\omega}{2}} \tag{4}$$

The Warburg impedance can thus be approximated by a resistance (R_a) in series with a parallel RC (R_w and C_w) circuit. On Fig. 2, R_p and R_a are combined into R_{eq}. Relationships between parameters of the model of Fig. 1 and parameters of the linear model of Fig. 2, derived from Eq. 4, are as follows : $\tau_d = 2R_wC_w$ and $R_d = R_{eq} + R_w$. Substituting the linear expression of the Warburg impedance of Eq. 4 for the non-linear one in Eq. 2 let us compute the following continuous

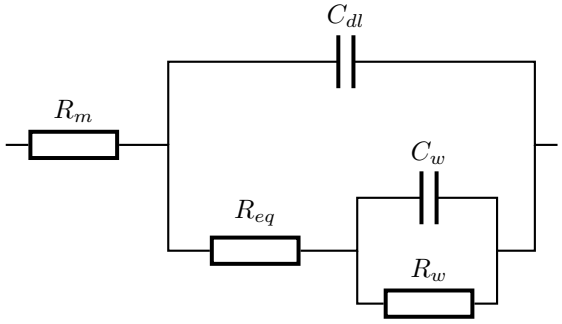

Fig. 2. Linear approximation of the Randles cell.

time transfer function :

$$F(s) = R_m + \frac{R_{eq} + R_w + R_{eq}R_wC_ws}{1 + (R_wC_w + R_{eq}C_{dl} + R_wC_{dl})s + R_{eq}R_wC_{dl}C_ws^2} \quad (5)$$

in which the input is the current drawn from the fuel cell and the output is the stack's voltage.

For the sake of simplicity, $F(s)$ will be written as follows:

$$F(s) = R_m + \frac{R_1 + R_2\tau_1 s}{1 + \tau_2 s + \tau_3^2 s^2} \quad (6)$$

with $R_1 = R_{eq} + R_w$, $R_2\tau_1 = R_{eq}R_wC_w$, $\tau_2 = R_wC_w + R_{eq}C_{dl} + R_wC_{dl}$ and $\tau_3^2 = R_{eq}R_wC_{dl}C_w$.

The discrete time transfer function is given by the Z transform of the inverse Laplace transform of $B_0(s)F(s)$, where $B_0(s)$ is a zero order hold :

$$G(z) = \mathcal{Z}\left(\mathcal{L}^{-1}\left(B_0(s)F(s)\right)\right) \quad (7)$$

$$= (1 - z^{-1}) * \mathcal{Z}\left(\mathcal{L}^{-1}\left(\frac{F(s)}{s}\right)\right) \quad (8)$$

With a and b the denominator's roots, the discrete time transfer function is :

$$G(z) = X_1 + X_2\frac{z-1}{z - e^{-aT}} + X_3\frac{z-1}{z - e^{-bT}} \quad (9)$$

where T is the sampling period and,

$$X_1 = R_m + \frac{R_1}{\tau_3^2 ab} \quad (10)$$

$$X_2 = \frac{1}{(a-b)\tau_3^2}(R_1/a - R_2\tau_1) \quad (11)$$

$$X_3 = \frac{1}{(b-a)\tau_3^2}(R_1/b - R_2\tau_1) \quad (12)$$

Writing Eqn. 9 in the traditional form of a transfer function, we eventually get the discrete time model of the fuel cell impedance :

$$G(z) = \frac{Y(z)}{U(z)} = \frac{a_2z^2 + a_1z + a_0}{z^2 - b_1z + b_0} \quad (13)$$

TABLE I
PARAMETERS OF THE CONTINUOUS AND DISCRETE MODELS AS A FUNCTION OF THE FUEL CELL SOH.

Param.	Nom.	Flo.	$\Delta_{Nom/Flo}$	Dry	$\Delta_{Nom/Dry}$
R_m	0.0042	0.0047	+11%	0.0097	+130%
R_{eq}	0.0063	0.0123	+95%	0.0111	+75%
R_w	0.0044	0.0291	+566%	0.0104	+137%
a_0	0.0038	0.0042	+11%	0.0087	+130%
a_1	-0.008	-0.009	+11%	-0.0184	+130%
a_2	0.0042	0.0047	+11%	0.0097	+130%
b_0	0.9524	0.9622	ϵ	0.947	ϵ
b_1	1.9523	1.9621	ϵ	1.947	ϵ

with,

$$a_2 = X_1 + X_2 + X_3 \quad (14)$$

$$a_1 = e^{-aT}(-X_1 - X_3) + e^{-bT}(-X_1 - X_2) - X_3 - X_2 \quad (15)$$

$$a_0 = X_1e^{-(b+a)T} + X_2e^{-bT} + X_3e^{-aT} \quad (16)$$

$$b_1 = e^{-aT} + e^{-bT} \quad (17)$$

$$b_0 = e^{-(b+a)T} \quad (18)$$

The study of the dependence of a_0, a_1, a_2, b_0 et b_1 on the original parameters R_m, R_{eq}, R_w, C_{dl} and C_w shows that each parameter of Eqn. 13 discrete model is a function of every parameter of Eqn. 5 continuous model. This mixing of parameters is an unavoidable side effect of the discretization process. It is also a major drawback as far as fault isolation is concerned. Table I shows that the parameters of the continuous time model exhibit large variations when failures occur. Moreover, each failure causes only two of the three resistances to vary. Namely, membrane drying out influences R_m and R_w while flooding influences R_{eq} and R_w. This guarantees that fault isolation is possible. On the contrary, parameters of the discrete model appears to be more robust to the occurrence of a fault : an 11% increase in the case of flooding could easily go unnoticed, given the natural uncertainty of experimental measurements [3]. Moreover, each parameter is equally affected by the fuel cell SOH. If fault isolation was to be implemented, it would only rely on the magnitude of the variations, instead of the magnitude and the subset of affected parameters.

B. Fitting algorithm

The first step is to write the discrete transfer function of Eqn. 13 as a recursive equation in which the output of the system at a given time step (y_k) is given as a function of the inputs (u_{k-i}) and outputs (y_{k-i}) at previous time steps :

$$y_k = b_1y_{k-1} - b_0y_{k-2} + a_2u_k + a_1u_{k-1} + a_0u_{k-2} \quad (19)$$

Let's write θ the array holding parameters, and ϕ the array holding the system's inputs and outputs :

$$\theta = \begin{pmatrix} b_1 & b_0 & a_2 & a_1 & a_0 \end{pmatrix}^T \quad (20)$$

$$\phi = \begin{pmatrix} y_{k-1} & y_{k-2} & u_k & u_{k-1} & u_{k-2} \end{pmatrix}^T \quad (21)$$

In a recursive least square algorithm, the estimates $\hat{\theta}$ are updated at each step, based on the error between the model

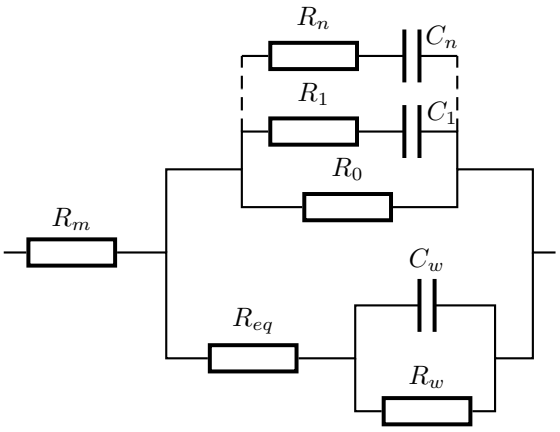

Fig. 3. Electrical circuit equivalent to Eqn. 30.

output and the predicted output $\hat{y}$:

$$\hat{\theta}_k = \hat{\theta}_{k-1} + L_k \left(y_k - \hat{y}_k\right) \tag{22}$$

The scheme can be viewed as a filter that averages the data to come up with optimal estimates. Averaging is a good strategy if model parameters are constant in nature. However, in the case of state-of-health monitoring, the parameters we are estimating are time varying and we want to keep track of variations. That is the concept of forgetting in which older data is gradually discarded in favor of more recent information. In least square method, forgetting can be viewed as giving less weight to older data and more weight to recent one. The objective function to be minimized is thus defined as follows :

$$J = \frac{1}{2}\sum_{i=1}^{k} \lambda^{k-i} \left(y_i - \phi_i^T \hat{\theta}_k\right)^2 \tag{23}$$

where λ is called the forgetting factor and $0 < \lambda \leq 1$. It operates as a weight which diminishes for the more remote data. The scheme is known as least-square with exponential forgetting and θ can be calculated recursively using the update equation 22. The update gain L_k is derived as follows :

$$L_k = P_{k-1}\phi_k \left(\lambda + \phi_k^T P_{k-1}\phi_k\right)^{-1} \tag{24}$$

where P_k is commonly refered to as the covariance matrix defined as :

$$P_k = \left(I - L_k \phi_k^T\right) P_{k-1} \frac{1}{\lambda} \tag{25}$$

More detailed derivation can be found in books on parameter estimation such as [12]. Proof of convergence is shown in [13].

C. Further theoretically possible improvements

So as to enhance the fault isolation capabilities of the model, it is tempting to try to improve the goodness of fit by reinstating the CPE in some way. When it comes to finding an integer order model equivalent to a CPE, R-C transmission lines are usually considered [14]. This approximation can either be seen as a purely mathematical trick, or as the true physical representation of some physical phenomena's spatial distribution, like the double layer charging for instance. It is out of the scope of this paper to discuss the physics behind the non integer behavior of the fuel cell. Furthermore, adding the R and C elements of the transmission line to the parameters to be fitted would greatly increase the number of degrees of freedom of the fitting algorithm and jeopardize any chance of success in that matter. therefore, the CPE approximation will be computed once and for all and no physical interpretation of the result will be attempted. The optimal approximation of the non-integer power of s used in the CPE transfer function is given by [15] :

$$s^p = G_0 \left(\frac{1+\frac{s}{\omega_l}}{1+\frac{s}{\omega_u}}\right)^p = G_0 \prod_{i=1}^{n} \frac{1+\frac{s}{\omega_i}}{1+\frac{s}{\omega_i'}} \tag{26}$$

where p is the derivation order, n the number of poles and zeros used in the approximation, G_0 a constant, ω_l and ω_u the lower and upper frequencies in-between which the approximation is valid. The relationship between two consecutive zeros or two consecutive poles in Eqn. 26 is given by :

$$\frac{\omega_{i+1}'}{\omega_i'} = \frac{\omega_{i+1}}{\omega_i} = \alpha\eta \quad \text{with} \quad \alpha\eta = \left(\frac{\omega_u}{\omega_l}\right)^{\frac{1}{n}} \tag{27}$$

the ratio between a pole and a zero and between a zero and the preceding pole are given by :

$$\frac{\omega_i}{\omega_i'} = \alpha \quad \text{and} \quad \frac{\omega_{i+1}'}{\omega_i} = \eta \quad \text{with} \quad \alpha = (\alpha\eta)^p \tag{28}$$

the first zero is given by $\omega_1' = \omega_l \eta^{1/2}$, the last pole by $\omega_n = \omega_u \eta^{-1/2}$. Lastly, the G_0 constant is defined as :

$$G_0 = \left(\frac{\omega_0}{A}\right)^p \quad \text{with} \quad \omega_0 = \sqrt{\omega_l \omega_u} \quad \text{and} \quad A = \left|\frac{1+j\frac{\omega_0}{\omega_l}}{1+j\frac{\omega_0}{\omega_u}}\right| \tag{29}$$

The fuel cell's impedance thus becomes :

$$Z(s) = R_m + \frac{1}{QG_0 \prod_{i=1}^{n} \frac{1+\frac{s}{\omega_i}}{1+\frac{s}{\omega_i'}} + \frac{1}{R_{eq}+\frac{1}{C_w s+\frac{1}{R_w}}}} \tag{30}$$

So as not to increase the fuel cell model's order, a development using two poles and two zeros is first computed. As shown in Fig. 4, the resulting model does not significantly improve the goodness of fit. The simulated high frequency resistance is closer to the measured one, but the model does not follow the high frequency lobe in an acceptable manner, and the transition between the two lobes is misplaced.

Figure 4 shows that in order to obtain a good agreement between experimental data and a linear integer order model, a tenth order approximation of the CPE is needed. Between 0.02Hz and 20kHz, the fractional derivative is approximated by the following transfer function :

$$\begin{aligned} s^{0,8} \approx & \frac{2,6.10^{-19}s^{10}+1,2.10^{-14}s^9+1,2.10^{-10}s^8+\ldots}{4,1.10^{-24}s^{10}+5,9.10^{-19}s^9+1,7.10^{-14}s^8+\ldots} \\ & \frac{2,8.10^{-7}s^7+1,6.10^{-4}s^6+2,3.10^{-2}s^5+\ldots}{1,2.10^{-10}s^7+2,1.10^{-7}s^6+9,3.10^{-5}s^5+\ldots} \\ & \frac{8,4.10^{-1}s^4+7,6s^3+17,2s^2+9,256s+1}{1,0.10^{-2}s^4+2,8.10^{-1}s^3+1,9s^2+3,1s+1} \end{aligned} \tag{31}$$

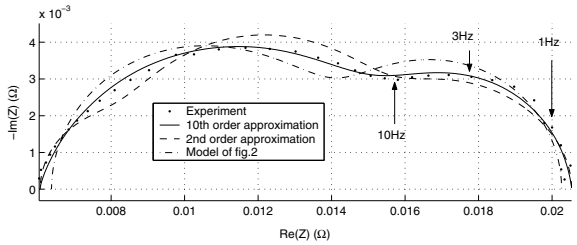

Fig. 4. Quality of the approximation as a function of the model order.

The coefficients of the transfer function of Eqn. 31 are computed once and for all given a frequency range and a non integer order. therefore, the fitting problem theoretically remains the same, with five degree-of-freedom . However, using Eqn. 31 in the expression of the fuel cell impedance raises practical issues. The model is now tenth order, which requires more computational power. Moreover, the five parameters we are interested in are going to be scattered across the twenty coefficients of the final transfer function without guarantee that this will improve in any way the ability to perform the diagnosis.

IV. FITTING IN THE FREQUENCY DOMAIN

Another approach consists in performing the data fitting in the frequency domain. This would allow us to keep working with the non linear form of the fuel cell impedance. Parameters would thus retain their physical meaning and sensitivity to the stack's flooding or drying out. The main drawback is that a time window has to be used for conversion from the time domain to the frequency domain using the Fourier transform. As a consequence, the fuel cell SOH estimation is not strictly real-time anymore since it is now delayed by the size of this window added to the time needed to process the data contained in the window. However, one of the challenge in Fault Detection and Isolation is to make sure that the diagnosis is available in due time to avoid irreversible damage to the system. In-house studies showed that both flooding and drying out take a few to several minutes before driving the fuel cell into a critical situation. therefore, being able to update the diagnosis every few seconds will be deemed sufficiently close to real time to allow for integration within the control loop, and for counter measures to be ready in time.

In conventional frequency domain EIS, the system under study is sequentially probed by pure sinusoidal waveforms of various frequencies. A signal generator is thus needed, which is hardly an on-board solution, and the cumulated time required to record a full spectrum is usually somewhere between five to ten minutes, depending on the frequency range and accuracy level.

We will address both these issues by using Fourier transform EIS [16] in order to use waveforms that can be found in on-board applications and a model-based complex non-linear least square fitting scheme so as to reconstruct the impedance spectrum from as few data as possible.

A. Impedance spectrum reconstruction

The concept of time resolved EIS is to combined into a single signal all the frequencies that we are interested in. It is therefore theoretically possible to obtain, in much less time, the same information on the system than with traditional EIS. A discrete Fourier transform lets us compute the voltage signal in the frequency domain, U_i, from the sampled time domain signal U_k :

$$U_i = \sum_{k=0}^{N-1} U_k \exp\left(-\frac{2j\pi ik}{N}\right) \tag{32}$$

The current signal I_i has a similar form. The real and imaginary impedances of the fuel cell are then determined from the voltage, current and phase data :

$$Z_{r,i} = \left|\frac{U_i}{I_i}\right| \cos\left(\arg U_i - \arg I_i\right) \tag{33}$$

$$Z_{j,i} = \left|\frac{U_i}{I_i}\right| \sin\left(\arg U_i - \arg I_i\right) \tag{34}$$

The overall performance of this method depends upon the frequency content of the current waveform and the width of the time window.

Choosing the size of the window results from a trade off between the lowest frequency that one wishes to record and the time that one is willing to wait before a diagnosis is available. In order for the fitting algorithm to succeed, the set of data which is passed to it has to contain a minimum amount of information giving a good description of the impedance spectrum. In our particular case, impedance spectra are made of two imbricated semi-circles, with respective sizes varying depending on the SOH [3]. An ideal data set would be one in which points are evenly distributed over the two semi-circles. Figure 4 shows an impedance spectrum recorded between 1kHz and 0.1Hz. The transition between the two lobes occurs around 10Hz. The top of the second lobe is reached around 3Hz, and at 1Hz, the impedance is halfway back toward the real axis. Knowing that it usually takes a few periods to gather enough information for an accurate spectral analysis to be performed, the 1Hz point is likely to take too much time to be recorded given our quasi real time objective. 3Hz will thus be the lowest frequency recorded.

Once the lowest frequency is set, higher frequency points are computed based on the harmonics present in the signal. Fortunately, the square signal, which is one of the richest signals in term of frequency content happens to be one of the most commonly encountered in an industrial environment. It has thus been selected for this study. With a fundamental frequency of 3Hz, the first harmonic will be at 9Hz, that is, right at the transition between the two lobes. Only one point on the low frequency semi-circle will therefore be available to the fitting algorithm.

On Fig. 5, the reconstructed spectrum is compared to one recorded with a Gamry® FC350 impedancemeter. As can be seen, the accuracy of FT-EIS is well in range with traditional EIS since both spectra are almost perfectly superimposed.

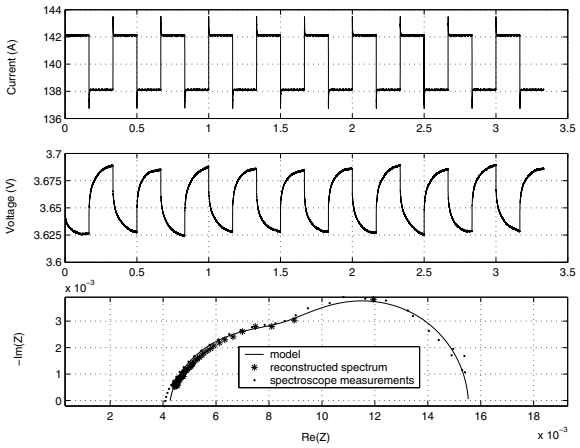

Fig. 5. Reconstruction of the impedance spectrum from 10 periods of a 3Hz square signal.

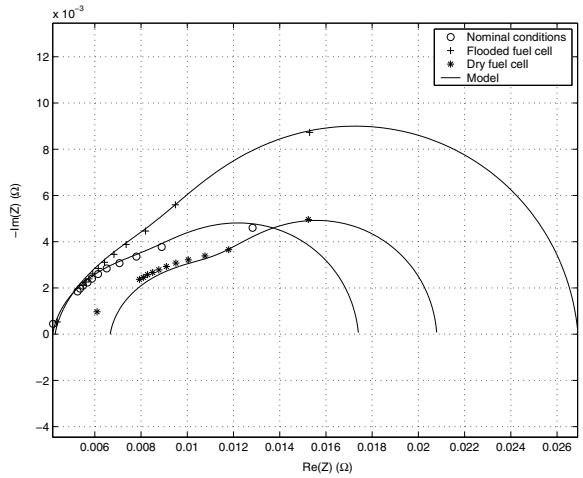

Fig. 6. Measured impedances and reconstructed spectra in nominal, dry and flooded conditions.

B. Fitting algorithm

A Levenberg-Marquardt non linear least square algorithm is used to fit the parameters. In that scheme the steepest descent method, which is used when far from the solution, is continuously replaced by a Gauss-Newton method as the estimation closes in on the objective function minimum [17]. This method has been proven to work in a wide array of real world applications and is a *de facto* standard in non-linear fitting. In our case, the choice of the objective function to be minimized is of great importance. Proper balance must be achieved between the high frequency part of the spectrum for which several data points are available and the low frequency part for which only one is. Dividing the impedance by the frequency let the low frequency data contribute a greater amount to the regression. Furthermore, it appears that the average ratio between real and imaginary parts of the fuel cell impedance is approximatively 3. Based on these considerations, we chose an objective function to be minimized by the regression algorithm of the following form :

$$J = \frac{1}{2}\sum_{i=1}^{N}\left[\left(\frac{Z_{r,i}-\hat{Z}_{r,i}}{\omega_i}\right)^2 + 9\left(\frac{Z_{j,i}-\hat{Z}_{j,i}}{\omega_i}\right)^2\right] \quad (35)$$

Alternative weighting strategies can be found in [18].

On Fig. 5 results of the fitting procedure, superimposed in solid lines on the bottom graph, show that the Levenberg-Marquardt algorithm succeeds in reconstructing the impedance spectrum, both in high and low frequencies. Results given in Fig. 6 for flooded, dry and nominal conditions show equally satisfying performance.

V. EXPERIMENTAL VALIDATION

A. Experimental setup

All measurements were carried out on a stack fed with air and pure hydrogen. So as to ensure stability and homogeneity of the fuel cell under test, active areas below 5cm^2 [19], [20], or single cells [21] are usually chosen for AC impedance measurements. To the knowledge of the authors, the largest active area investigated by means of electrochemical impedance spectroscopy and published to date is 50cm^2 [22]. In an attempt to come one step closer to a full size stack, a 6-cell assembly with an active area of 220cm^2 was selected for this study. Impedance spectra were computed based on the stack voltage. It introduced a fair amount of inhomogeneity and instability in the system, which, in turn, showed the robustness of the approach. Both flooding and drying out were triggered on-line, by changing the inlet gas relative humidity.

Fuel cell's operating conditions were monitored and controlled through a Greenlight Power® FCATS-L test station. Signal generation and acquisition were done using a National Instrument® PCI-6221 board connected to a RBL232 50-400-2000 loadbox from TDI Dynaload®. The fuel cell was directly connected to the load. therefore, the anode acts as the reference electrode. During the experiment, temperature was maintained at 80C, stoichiometries at 1.5 on anode's side and 2 on cathode's side and the fuel cell stack was operated at 1.5 bara on both sides. The highest frequency of interest to our study was set to 1kHz. Wires' inductive behavior was predominant above that frequency. The sampling rate was set to 20kHz, and seventh order analog anti-aliasing filters with a cut-off frequency of 2kHz were used. Such an oversampling procedure ensures an attenuation of -96dB at the Nyquist frequency of 10kHz, as well as a small anti-aliasing filter induced phase shift at 1kHz.

The probing signal is a 3Hz, 4A peak-to-peak square waveform. In the case of temporal fitting, it is continuously applied. In the case of frequency domain fitting, it is applied for ten periods. This solicitation represents a little less than 3% of the total power delivered by the fuel cell. Although being small it clearly cannot be neglected. In the case of a hybrid transmission, this solicitation could come from batteries or super-capacitors for instance. Ideally, natural solicitations of the fuel cell by the system's ancillaries would be enough for the fitting algorithm to operate.

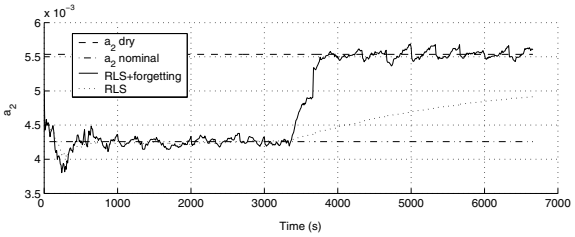

Fig. 7. Time domain fitting of a_2 in nominal and dry conditions.

B. Temporal domain scheme

Performances of this fitting scheme were assessed offline, on experimental data. Figure 7 shows the result of the parameter a_2's fitting during a two hour long test in which the fuel cell was successively operated in nominal and dry conditions. Adding the forgetting factor allows an efficient tracking of the parameter's variation, which is impossible with the regular recursive least square scheme. Fitting of the other parameters behave in the same way. In regard with the poor isolation properties that can be expected from this scheme, it has not been any further developed in this study.

C. Frequency domain scheme

Figure 8 shows the mean cell voltage of the stack during a one hour and fifteen minutes long experiment in which the stack was successively operated in dry, nominal and flooded conditions. The DC current was kept constant for the whole duration of the test, so as to ensure that the state of health of the fuel cell is solely responsible for the voltage variation. As can be seen, the occurrence of a fault results in a voltage drop representing 10% of the initial value. In the case of membrane drying out, the six cells of the stack are affected in an identical way. Cell voltages thus remain rather high and short to mid-term integrity of the stack is not threatened. This information is nonetheless interesting in view of stack durability and performance optimization. On the other hand, flooding only affects one cell, which drops to voltages as low as 0.2V. Such a low voltage is beyond the range of safe operation, and can lead to irreversible damage. Diagnosis should thus be reliable and counter measures must be quickly devised.

On figure 9, symbols represent triplets (R_m, R_p, R_d) fitted to experimental data. Circles were drawn to indicate subspaces in which the fuel cell will be considered in nominal, dry or flooded condition. The fuel cell was probed once every minute for the duration of the experiment.

Circles correspond to the first part of the experiment during which the fuel cell is drying out, between 1 and 1300 seconds. Asterisks correspond to the second part in which the fuel cell comes back to nominal condition, between 1300 and 2000 seconds. Finally, plus signs correspond to the third part during which the fuel cell gets flooded before going back again to nominal condition, between 2000 and 4500 seconds. Letters also indicate correspondence between the temporal graph and 3D graph. On this last graph, flooded and dry operation of the fuel cell are easily distinguishable, each one having its own

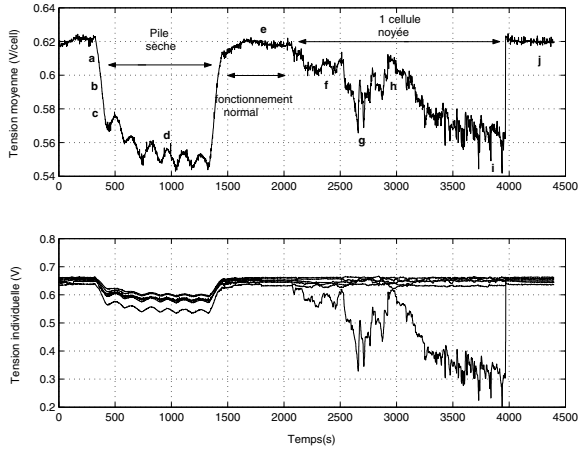

Fig. 8. Stack and single cell voltages as a function of time and state-of-health.

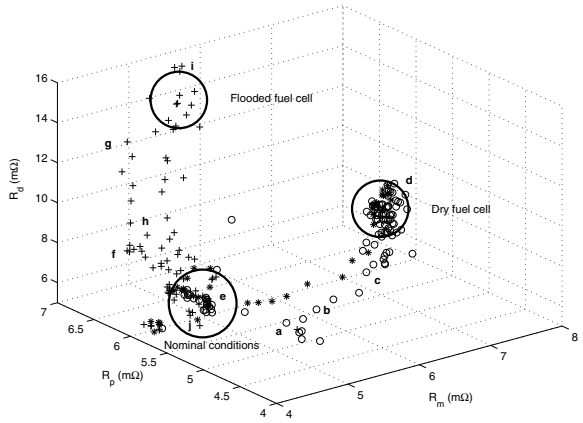

Fig. 9. Evolution of the fuel cell SOH during the experiment shown in Fig. 8.

subspace sufficiently distant from each other to ensure that a decision making algorithm will produce a reliable diagnosis.

VI. CONCLUSION

On the one hand, working in the time domain ensures true real time performance through the use of a recursive fitting algorithm. Unfortunately, linearization and discretization causes the model to partially loose its ability to isolate failures. Trying to improve the goodness of fit through the approximation of the CPE yielded complex models.

On the other hand, working in the frequency domain allowed for the use of the non-linear model, in which parameters have a strong physical meaning and great sensitivity to flooding and drying out of the fuel cell. On the downside, a time window has to be used, thus delaying the availability of the diagnosis. It has been shown that 10 periods of a 3Hz square signal carried enough information in order for the full impedance spectra to be accurately reconstructed by a non-linear Levenberg-Marquardt algorithm. Reliable monitoring of flooding and drying out was experimentally demonstrated using this method. Quasi real time performances were achieved with the possibility to update the diagnosis every

three seconds. It is our belief that the improvement in isolation capabilities is worth this delay.

Further investigation include the study of the influence of fuel cell aging and cathode poisoning on the ability to detect and isolate flooding and drying out.

REFERENCES

[1] V. Venkatasubramanian, "Process fault detection and diagnosis : past, present and future," in *Proceedings of the 4th workshop on on-line fault detection and supervision in the chemical process industries*. Jejudo Island, South Korea: IFAC, 2001.

[2] R. Eckl, W. Zehtner, C. Leu, and U. Wagner, "Experimental analysis of water management in self-humidifying polymer electrolyte fuel cell stack," *Journal of Power Sources*, vol. 138, pp. 137–144, 2004.

[3] N. Fouquet, C. Doulet, C. Nouillant, G. Dauphin-Tanguy, and B. O. Bouamama, "Model based pem fuel cell state-of-health monitoring via ac impedance measurements," *Journal of Power Sources*, 2006, in Press.

[4] S. Knights, K. Colbow, J. St-Pierre, and D. Wilkinson, "Aging mechanisms and lifetime of pefc and dmfc," *Journal of Power Sources*, vol. 127, pp. 127–134, march 2004.

[5] K. Tüber, D. Pózca, and C. Hebling, "Visualisation of water build up in the cathode of a transparent pem fuel cell," *Journal of Power Sources*, vol. 124(2), pp. 403–414, november 2003.

[6] M. Mench, Q. Dong, and C. Wang, "In situ water distribution measurements in a polymer electrolyte fuel cell," *Journal of Power Sources*, vol. 124(1), pp. 90–98, october 2003.

[7] A. Tsukada, E. Lehmann, P. Vontobel, and G. Sherer, "In situ observation of water condensation in an operating polymer electrolyte fuel cell by means of neutron imaging at the spallation neutron source (sinq)," Paul Sherrer Institute, Tech. Rep., 1999.

[8] W. He, G. Lin, and T. Nguyen, "Diagnostic tool to detect electrode flooding in proton exchange membrane fuel cells," *AIChE Journal*, vol. 49(12), p. 3221, 2003.

[9] A. Bosco and M. Fronk, "Fuel cell flooding detection and correction," U.S. Patent 6,103,409, 2000.

[10] D. Hissel, M. Péra, and J. Kauffmann, "Diagnosis of automotive fuel cell power generators," *Journal of Power Sources*, vol. 128(2), pp. 239–246, april 2004.

[11] H. Girault, *Electrochimie physique et analytique*. Presses polytechniques et universitaires romandes, 2001.

[12] A. Astrom and B. Wittenmark, *Adaptive control*. Addison Wesley, second edition, 1994.

[13] S. Bittani, P. Bolzern, M. Campi, and E. Coletti, "Deterministic convergence analysis of rls estimators with different forgetting factors," in *Proceedings of the 27th conference on decision and control*. Austin, TX: IEEE, December 1988.

[14] S. Buller, M. Thele, E. Karden, and R. deDoncker, "Impedance-based non-linear dynamic battery modeling for automotive applications," *Journal of Power Sources*, vol. 113, pp. 422–430, 2003.

[15] A. Oustaloup, J. Sabatier, and P. Lanusse, "From fractal robustness to the crone control," *Fractional Calculus and Applied Analysis : An International Journal for Theory and Applications*, vol. 2, 1999, n1.

[16] J. Garland, C. Petit, and D. Roy, "Analysis of experimental constraints and variables for time resolved detection of fourier transform electrochemical impedance spectra," *Electrochimica Acta*, vol. 49, p. 2623, 2004.

[17] K. Madsen, H. Nielsen, and O. Tingleff, "Methods for non-linear least squares problems," Technical University of Denmark, Tech. Rep., 2004.

[18] M. Orazem, P. Agarwal, and L. Garcia-Rubio, "Critical issues associated with interpretation of impednce spectra," *Journal of Electroanalytical Chemistry*, vol. 378, pp. 51–62, 1994.

[19] V. Paganin, C. Oliveira, E. Ticianelli, T. Springer, and E. Gonzalez, "Modelistic interpretation of the impedance response of a polymer electrolyte fuel cell," *Electrochimica Acta*, vol. 43, pp. 3761–3766, 1998.

[20] X. Wang, I.-M. Hsing, Y.-J. Leng, and P.-L. Yue, "Model interpretation of electrochemical impedance spectroscopy and polarization behavior of h_2/co mixture oxidation in polymer electrolyte fuel cells," *Electrochimica Acta*, vol. 46, pp. 4397–4405, 2001.

[21] T. Abe, H. Shima, K. Watanabe, and Y. Ito, "Study of pefcs by ac impedance, current interrupt, and dew point measurements. i : Effect of humidity in oxygen gas," *Journal of The Electrochemical Society*, vol. 151(1), pp. A101–A105, 2004.

[22] R. Makharia, M. Mathias, and D. Baker, "Measurement of catalyst layer electrolyte resistance in pefcs using electrochemical impedance spectroscopy," *Journal of The Electrochemical Society*, vol. 152(5), pp. A970–A977, 2005.